Impact of salt and frost weathering on the physical and durability properties of travertines and carbonate tufas used as building material

D. Benavente · J. Martinez-Martinez[1,2] · N. Cueto[1] · S. Ordoñez[1] · M. A. Garcia-del-Cura[3]

[1] Departamento de Ciencias de la Tierra y del Medio Ambiente, Universidad de Alicante, Campus San Vicente del Raspeig, 03690 San Vicente del Raspeig, Alicante, Spain

[2] Instituto Geológico y Minero de España (IGME), Calle Ríos Rosas, 23, 28003 Madrid, Spain

[3] Instituto de Geociencias (IGEO) (CSIC-UCM), C/José Antonio Novais, 12, 28040 Madrid, Spain

Abstract

This study aims to understand the effect of salt and frost crystallisation on the petrophysical and durability properties of representative types of travertine and carbonate tufas. Results demonstrate that the studied travertines and tufas exhibit a very high durability against salt and ice crystallisation cycles, compared to carbonates rocks with similar porosity values. The variation of the loss of mass, effective porosity, capillary absorption coefficient, ultrasonic wave velocity and attenuation, and compressive strength was scarce during weathering tests. The evolution of petrophysical properties was slightly more intense after 30 cycles of salt crystallisation than 100 cycles of freeze–thaw. Petrophysical and durability properties of the travertines and carbonate tufas depend on porosity fraction and on the manner in which the vuggy porosity is connected. In the travertine facies, vuggy macropores show little connection and can be considered as separate-vug porosity. Their addition to interparticle porosity increases effective porosity and reduces their mechanical strength but does not significantly increase capillary transport and the effectiveness of salt and ice action over the stone. On the contrary, in the carbonate tufas, vugs act as touching-vug pores, as capillary imbibition coefficients reveal. However, scanning electron microscopy displays that they underwent microcracking processes related mainly to both thermal stresses and/or ice and salt pressures. These microcracks present little connection, and they do not enhance noticeably the water flow or decrease the mechanical properties. These results are finally discussed in terms of a nonlinear decay pattern, which with long periods of apparent stability might be followed by rapid and catastrophic decay.

Keywords Travertine · Carbonate tufa · Salt weathering · Freeze–thaw cycles · Building stones

Introduction

Travertine is worldwide employed as building stone for monuments and civil constructions from ancient times until present (Pentecost 2005). It has been used as structural stone and also in ornamental elements such as sculptures. Travertine is commonly seen in tile sizes as façade material, wall cladding and flooring (Demirdag 2013; Chentout et al. 2015). Tufa has been used as dimension stone commonly in vernacular architecture (Pedley 2009; Unterwurzacher et al. 2010; Garcia-del-Cura et al. 2014).

The term travertine comes from the Latin "*Lapis tiburti-nus*" and was widely used by the Romans from ancient times (Vitruvio, in "*The Architectura and Pliny the Elder in Naturalis Historia*" (Curie 2013). The Romans used the term tophus (tufa) for any freshwater carbonate developed under ambient temperature conditions. Generally, tufas are associated with abundant fossil moulds and casts of plants

and trees which represent the vegetation which originally grew around lakes, rivers and hill slopes where the deposit formed (Pedley 2009).

According to Pentecost and Viles (1994), the term travertine is known as thermogene travertine. It has been widely used for hydrothermal precipitates from warm to hot waters or formed with CO_2 from endogenous processes. The term tufa is adapted for metheogene travertine. It is used to indi-cate a powdery rock, and it is related to cool water deposits or CO_2 of the soil and epigean origin. In some formations, in fact, tufas and travertines may coexist in lacustrine limestone deposits (Garcia-del-Cura et al. 2012). Although the terms tufa and travertine are often used indiscriminately (Pedley 2009), their structural features and petrophysical properties are entirely different. Whereas travertines present parallel structures, tufas display a high diversity of macrophyte casts (Ford and Pedley 2006).

Previous studies have shown travertine is a relative dura-ble stone (Yavuz and Topal 2007; Yu and Oguchi 2010; Török and Vasarhelyi 2010; Akin and Özsan 2011; Zalooli et al. 2017), although few studies have been performed on carbonate tufas. In outdoor environments, they can undergo significant physical weathering due to salt crystallisation, freeze–thaw and/or thermal shock action, depending on the regional climate. In carbonate rocks as travertines and tufas, thermal stress may become determinant under daily ther-mal cycles because calcite has a highly anisotropic thermal dilatation (Nye 1972). Temperature fluctuations above and below freezing point or dissolution–precipitation boundary yield mechanical pressures by ice and salt crystallisation into pore space. There is, therefore, a feedback between both thermal and ice and salt crystallisation decay mechanisms.

Despite the extensive use of travertines as a building material, very few studies have been conducted to deter-mine the influence of the structures of travertines and tufas on their durability behaviour. The aims of this paper are (1) to study the influence of travertines and tufas structures on their petrophysical properties described as effective porosity, capillary absorption coefficient, ultrasonic wave velocity and attenuation, and compressive strength, and (2) to quantify the response of the travertines and carbonate tufas to salt and ice crystallisation by the evolution of their petrophysi-cal properties.

Materials and methods

Stone types

The studied travertines and carbonate tufas are used now-adays as building materials or found in the Spanish built heritage.

Spanish building stones have been quarried in Albox and Alhama de Almería (Almería province, SE of Spain). They are compared with the Turkish travertine, widely marked in Spain and aesthetically similar to white Classic Roman Travertine (Garcia-del-Cura et al. 2012; Zalooli et al. 2017). The extracted tufas and travertines from the different quarries present different types of the facies described above. There is no direct relationship between their textures and structures and the extracted travertine and tufa in each quarry. For example, non-porous cryp-tolaminated travertine facies can be found in Albox and Alhama de Almería quarries. On the other, in the Alhama de Almería quarry, both travertines and homogeneous tufas are present and the main travertines facies are NPM and Lmix.

Travertines of the Albox and Alhama de Almería quarries were generated by hot water springs associated with hydrothermal activity along the Betic Cordillera fault (Garcia-del-Cura et al. 2017). These travertines are col-oured (brownish-reddish) stones by the presence Fe–Mn oxyhydroxides (Garcia-del-Cura et al. 2007, 2008). The commercial name for the travertines extracted from Albox quarry is Yellow Gold Travertine (Travertino Oro), whereas travertines from Alhama de Almería quarry are known as Red Alhama (Rojo Alhama) (Garcia-del-Cura et al. 2008) and Olivillo (Urosevic et al. 2010).

According to Choquette and Pray classification of porosity (Choquette and Pray 1970), the studied travertines and tufas show mainly intercrystalline porosity. Intergran-ular porosity is scarce and is only present in some samples of complex tufas and laminated and massive travertines facies with thick layers. Intergranular porosity is associ-ated with the presence of pellets, intraclasts, etc. Inter-crystalline porosity is related to micrite, with a pore size of 0.005–0.05 μm, and large crystals with the pore size in the interval of 0.05–2 μm.

The main macroporosity of travertines is the fenestral porosity, which can achieve centimetric-size pores. In some laminated travertine samples, bacterial shrubs tex-tures present framework porosity. The direction of growth of framework pores is perpendicular to the sedimentary structure in these samples. The fenestral porosity in trav-ertines can be considered as separate-vug porosity, accord-ing to Lucia's petrophysical classification of pores (Lucia 1995). Pore connectedness is enhanced in the direction parallel to the bedding and also by the presence of micro-karstics processes in the stone. In carbonate tufas, plants casts are the most important macropores, which have an easy connection and they act as touching-vug pores. The presence of vuggy macropores in samples is highly hetero-geneous and changes from sample to sample.

Petrophysical properties

The petrophysical and durability characterisation were carried out in 150 samples of travertines and carbonate tufas. Salt crystallisation and freeze–thaw tests were performed to evaluate their durability. Pore structure was only measured on unaltered samples to describe the petrophysical and dura-bility behaviour of studied rocks. The petrophysical proper-ties were: effective porosity, capillary imbibition, *P*-wave velocity and spatial attenuation of the ultrasonic waves and uniaxial compressive strength. The characterisation of porosity, capillary imbibition and ultrasonic parameters were performed with non-destructive protocols, so they were also measured during durability tests in order to evaluate the changes in rock properties.

Pore structure was characterised using mercury intrusion porosimetry and complemented with the digital analysis of scanned samples. Connected porosity and pore-throat size distribution were calculated using an Autopore IV 9500 Micrometrics mercury porosimeter (MIP) with a pore size interval of 0.002–200 μm. Image analysis of scanned sam-ples was performed with JMicrovision (Roduit 2007) and was used to evaluate the large pore fraction that MIP cannot measure. Effective porosity, P, was determined using the vacuum water saturation test (UNE-EN 1936 2007). Dried samples were weighed and placed in a vacuum chamber at 20 ± 7 mbar in order to eliminate any trapped air from the porous systems. Distilled water was slowly introduced until the samples were completely covered, and finally, atmospheric pressure was re-established. The saturated and immersed weight of each sample was recorded.

The capillary absorption coefficient, C, was determined using the standard method in accordance with UNE-EN 1925 (1999). The continuous method was used to charac-terise tufa varieties because of their high absorption rates ($C > 150$ g/m^2 s$^{0.5}$) (Benavente et al. 2007a). Capillary imbibition was performed in both parallel and perpendicular direction. The capillary anisotropy coefficient, A_C, quantifies the anisotropy of the capillary flow and is defined as the ratio between lowest and highest capillary absorption coefficients. The dimensionless anisotropic coefficient has a maximum value of one for isotropic rock, and it decreases as sample anisotropy increases.

Ultrasonic waves were measured using a signal emitting–receiving equipment (Panametrics-NDT 5058PR) and an oscilloscope (TDS 3012B-Tektronix). *P*-wave propagation velocity, v_P, and spatial attenuation, α_s, were obtained with a *P*-polarised transducer of 1 MHz. The v_P anisotropy coefficient, A_{vp}, quantifies the anisotropy of *P*-wave veloci-ties in parallel and perpendicular directions and is defined as the ratio between lowest and highest v_P values. As in the capillary anisotropy coefficient, A_{vp} ranges from 0 to 1 and reaches the maximum value for isotropic rocks. The uniaxial compressive strength, σ_C, was performed according to the standard test EN 1926 (2007) using an Ibertest MEH-2000 H/FIB-50.

Durability tests

Salt crystallisation and freeze–thaw tests were in concordance with EN-12370 (1999) and EN-12371 (2011) recommendations, respectively. In order to evaluate the response of samples to prolonged salty aggressive environments, 30 cycles were carried out in the salt crystallization test, cor-responding to two consecutive normalised tests (15 cycles each one); 5-cm cubic samples of each lithotype were tested and underwent cycles of saline immersion (14% w/w Na_2SO4 solution, at 20 °C for 4 h), drying (at 60 °C for 16 h) and cooling at room conditions (20 °C, for 4 h). Samples were exclusively cleaned at the end of the test (after the 30 cycles). The evolution of the effective porosity, capil-lary imbibition, *P*-wave velocities and the dry weight loss, ΔW (%), was calculated at the 15th (uncleaned sample) and 30th cycles (after salt removal). The uniaxial compressive strength was also recorded in the 30th cycle.

Freeze–thaw test was carried out in a freezing chamber. The test consists of three parts: (1) temperature decreases to − 8 °C for 2 h without water addition in the freezing cham-ber (dry conditions); (2) temperature decreases to − 12 °C for 4 h (maintaining dry conditions); and (3) temperature increases to 20 °C, and freezing chamber is filled with the distilled water (wet conditions and sample water saturation). The evolution of effective porosity, capillary imbibition, *P*-wave velocities and the dry weight loss was recorded at 48, 75 and 100 durability cycles. Spatial attenuation was also measured in the last cycles (75 and 100th cycles), whereas compressive strength was finally performed in the 100th cycle. The number of samples with porous laminated traver-tines (PL) was not statistically representative, and therefore, these samples were not tested.

The specimens were visually inspected in order to evaluate the salt and ice action. Moreover, a small sample of each variety was observed under electron microscopy to evalu-ate microtextural changes produced during the durability test. Uncoated samples were analysed using a HITACHI S-3000 N microscope. The microanalysis was carried out with energy-dispersive X-ray (EDX) using an X-ray detector Bruker Xash 3001 working at 20 kV.

Results and discussion

Pore structure

The studied travertines present four types of facies, termed as non-porous massive travertine (NPM), banded or porous laminated travertine (PL), laminated with vugs

and non-porous levels (Lmix) and non-porous cryptolaminated trav-ertine (NPCL). Carbonate tufas have two facies, denomi-nated as homogeneous (HT) and complex tufas (CT).

Travertines and carbonate tufas are complex porous media, with wide-ranging porosity and pore size. Figure 1 shows the polymodal nature of the pore size distribution of the studied stones. Travertines and tufas present various pore types that describe different petrophysical and durabil-ity properties of the stones, such as vapour adsorption and condensation, capillary transport, mechanical strength and salt and ice crystallisation. Intercrystalline and intergranular porosity and some growth framework porosity are poorly sorted and range between 0.01 and 10 μm, although pore sizes of intergranular porosity are larger and better selected than intercrystalline pores. Vuggy porosity presents pore sizes up to 100 μm and can achieve centimetric-size pores. In the travertine facies, vuggy macropores show little con-nection and can be considered as separate-vug porosity.

Travertines and tufas have a wide dispersion of effec-tive porosities, mainly in carbonate tufa samples. Effective porosity of travertines is lower than for carbonate tufa sam-ples, although some complex tufas with less vuggy pores can reach porosity values lower than 10% (Table 1). The pres-ence of vuggy macropores in samples causes a discrepancy between effective and capillary porosity, as a result of their heterogeneity, connectedness and large size. Garcia-del-Cura et al. (2012) observed the same behaviour when the porosity obtained from MIP was compared with effective porosity results.

Figure 1 also displays the influence of pore size in vapour adsorption and condensation. Although they were not obtained in this study, their role in stone weathering may be crucial. Thus, a porous rock with high capacity and susceptibility to water condensation and retention into the material is more prone to deterioration by salt and ice crystallisation, chemical deterioration or the development of microorganisms (Sanchez-Moral et al. 2005; Benavente 2011; Benavente et al. 2011). At low relative humidities (first stages of the condensation process), vapour water is adsorbed on pore surface of the stone. With rising air humid-ity, the number of layers of water molecules on the pore sur-face increases until capillary condensation occurs for pore radius around 0.1 microns.

Water transport properties

Water transport by capillary imbibition reflects the porosity, pore size and pore connectivity of vuggy porosity of trav-ertines and tufas. For capillary coefficients, massive facies (NPM) registered the lowest values, whilst homogeneous (HT) and complex porous tufa (CT) facies showed the high-est values (Table 1).

Figure 1 displays the pore sizes in which the capillary flow is active. Capillary imbibition occurs mainly in pore size range between 1 μm and 1 mm and provides high water absorption rates for a well-connected pore structure. Inter-particle pore connectivity increases with porosity and tends to be reached for homogeneous porous rocks with porosity values higher than 10% (Benavente et al. 2007a, 2015). Fig-ure 2a shows a change in the tendency between porosity and capillary coefficient for porosity values up to 10%.

In tufa facies, macropores act as touching-vug pores, which explain the high values of the connected porosity and capillary imbibition coefficients (Table 1). In this context, Garcia-del-Cura et al. (2012) observed these macropores play a decisive role in water-weight uptake when they are well interconnected with interparticle micropores and do not exceed ~ 3 mm in diameter. Fluid movement by capillar-ity up to this pore size would be negligible, and the most important mechanism would be gravitational. Travertine facies, and particularly in laminated facies, present a strong anisotropy. C is much higher in the direction parallel to the bedding, where vugs connectivity increases within the stone lamination. Capillary anisotropy coefficient, A_C, features this behaviour and is sensible to micro- and macrostructure of the rocks (Table 1).

Ultrasonic parameters

Figure 2c shows a negative linear relationship between *P*-wave velocity and porosity as pore fraction hinders prop-agation of ultrasonic waves. Similar values and tendencies for travertines are found in Akin (2010); Akin and Özsan (2011) Siegesmund and Dürrast (2011); Demirdag (2013); Chentout et al. (2015); and Soete et al. (2015). However, non-porous cryptolaminated travertines (NPCLs) present a different trend. According to Garcia-del-Cura et al. (2012), this travertine facies show a strong increase in v_P at small porosity increments, which is linked to crystal size and low intercrystalline porosity. NPCLs present a highly re-crystal-lised texture with high contents of sparite with crystal size ranging from 50 to 200 μm. This tendency is also found in crystalline carbonate rocks where rocks with large crystals present lower propagation velocity (Martinez-Martinez et al. 2011, 2016). The influence of laminated structures on v_P is less significant than in the capillary flow. v_P anisotropy coefficient, A_{vp}, is close to 1 for most of the studied samples, whereas mean values of capillary anisotropy coefficient, A_C, are in the interval of 0.14–0.73. Anisotropy in porous laminated travertines is slightly higher (lower A_{vp}) than it is in other facies, which present similar values (close to 1) and, therefore, do not reflect rock anisotropy. These results suggest that v_P is not the most suitable parameter for quan-tifying rock anisotropy, despite the fact that travertines are

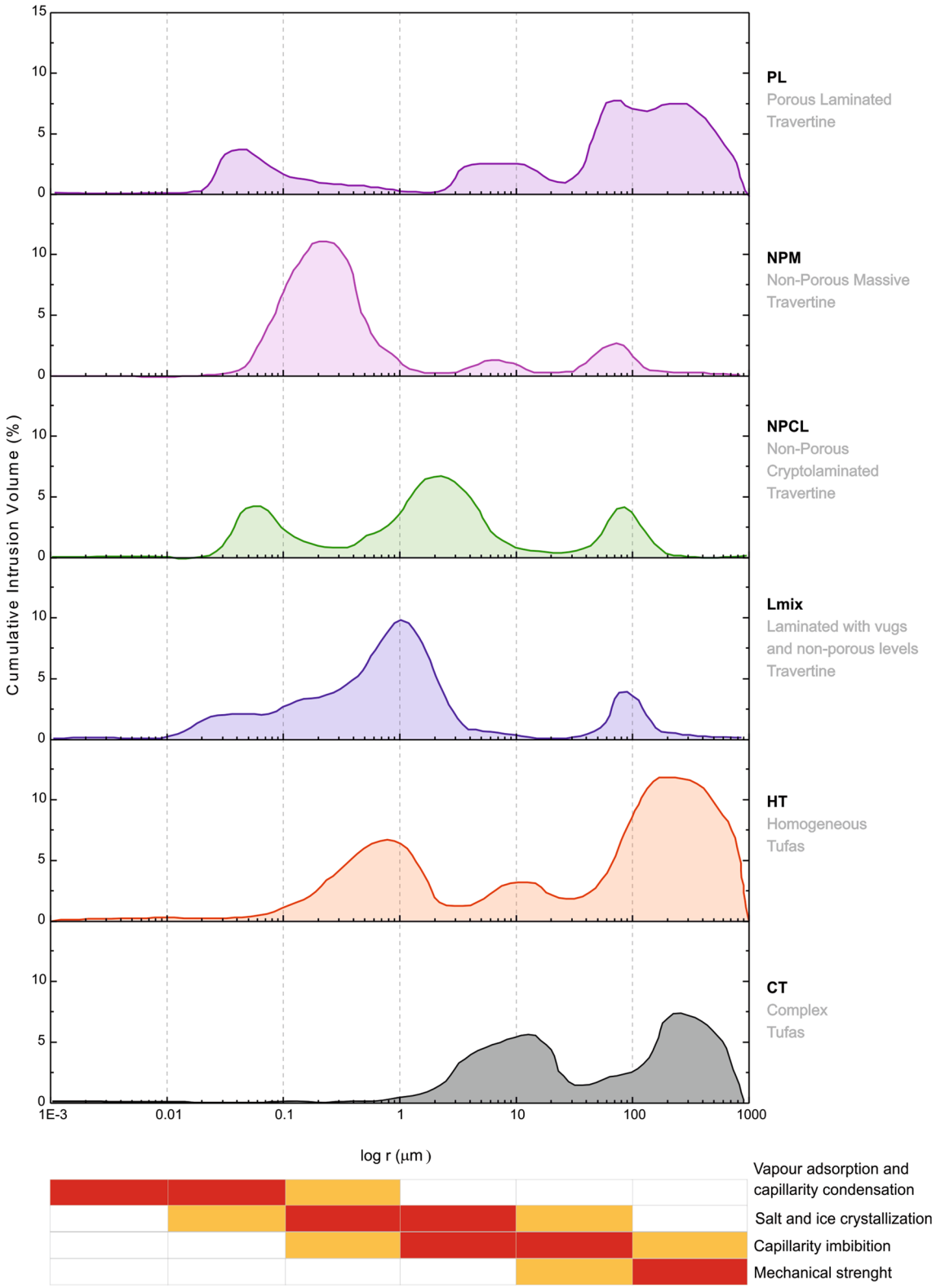

Fig. 1 Relationship between pore size distribution of the studied stones with vapour adsorption and condensation, salt and ice crystallisation, capillary transport and mechanical properties

Table 1 Petrophysical properties of unweathered samples

Facies	*n*	*P* (%)	C_{par} (g/m^2 s$^{0.5}$)	A_C	v_P (m/s)	A_{vp}	α_s (dB/cm)	σ_C (MPa)
CT	13	15.36 ± 7.61	20.75 ± 6.47	0.73 ± 0.21	5434 ± 387	0.97 ± 0.02	8.23 ± 3.75	40.20 ± 27.25
HT	10	37.49 ± 3.63	301.89 ± 133.61	0.27 ± 0.26	4164 ± 292	0.93 ± 0.03	13.14 ± 0.89	30.95 ± 10.29
Lmix	12	10.28 ± 3.60	6.37 ± 4.50	0.48 ± 0.16	5656 ± 293	0.93 ± 0.05	4.61 ± 1.44	58.91 ± 21.37
NPCL	10	7.17 ± 1.63	3.56 ± 2.00	0.52 ± 0.21	4014 ± 1199	0.89 ± 0.06	6.01 ± 0.77	42.74 ± 9.77
NPM	23	8.55 ± 2.08	5.22 ± 4.26	0.71 ± 0.29	5508 ± 163	0.96 ± 0.04	4.82 ± 0.65	37.67 ± 9.82
PL	6	22.84 ± 2.03	84.13 ± 66.35	0.14 ± 0.09	4727 ± 171	0.87 ± 0.06	9.14 ± 1.09	19.32 ± 3.30

Mean values and standard deviations for of the effective porosity. Facies: non-porous massive travertine (NPM), porous laminated travertine (PL), laminated with vugs and non-porous levels (Lmix) and non-porous cryptolaminated travertine (NPCL). Carbonate tufas have two facies, denominated as homogeneous (HT) and complex tufas (CT)

P capillary absorption coefficient in the direction parallel to the bedding, C_{par} capillary anisotropy coefficient, A_C ultrasonic wave velocity, v_P anisotropy coefficient of v_P, A_{vp} spatial attenuation, α_s compressive strength, σ_C and number of tested samples

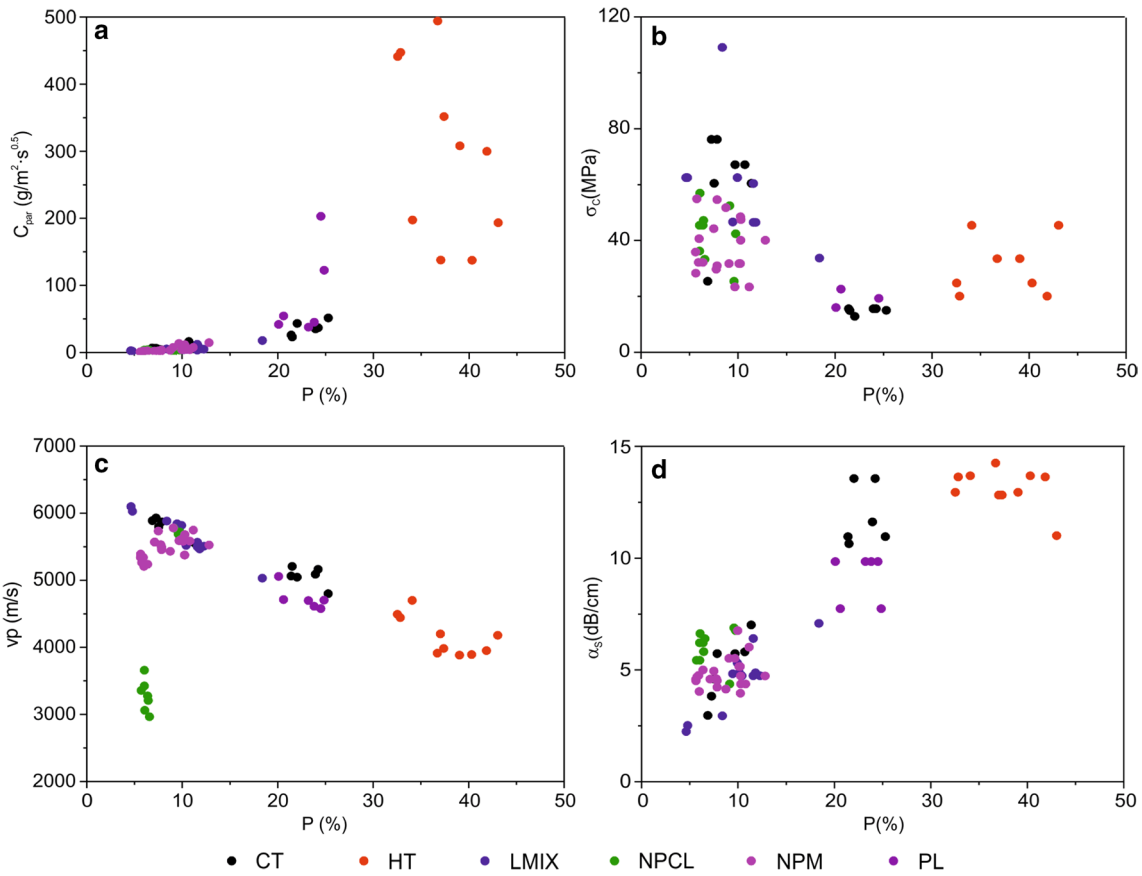

Fig. 2 Influence of porosity, *P*(%) on **a** capillary imbibition coef-ficient in the direction parallel to the bedding, C_{par}; **b** compressive strength, σ_C; **c** *P*-wave velocity, v_P; and **d** spatial attenuation, α_s. Facies: non-porous massive travertine (NPM), porous laminated travertine (PL), laminated with vugs and non-porous levels (Lmix) and non-porous cryptolaminated travertine (NPCL). Carbonate tufas have two facies, denominated as homogeneous (HT) and complex tufas (CT)

anisotropic rocks for the mechanical strength and capillary flow water.

Figure 2d displays a direct relationship between spatial attenuation and porosity. The presence of macropores causes high wave scattering compared to interparticle porosity. Thus, tufa facies show the highest α_s values and low-porous travertines show the lowest α_s. α_s and v_P are sensible to dif-ferent petrographic features. Martinez-Martinez et al. (2011, 2013) reported that spatial attenuation is much more sen-sitive to occasional rock defects (as vuggy macropores in travertines) than wave velocity. Therefore, the velocity of the wave front occurs through the more favourable fraction

of the rock, and therefore, v_P is less sensitive to the presence of these rock defects than α_S. Spatial attenuation depends slightly on crystal size contrarily what is observed to wave velocity. Thus, non-porous cryptolaminated travertines (NPCLs) show α_S values in concordance with their porosity (Garcia-del-Cura et al. 2012).

Mechanical properties

Travertines and tufas present a low-to-medium resistance according to Deere and Miller (1966) and range from 20 to 75 MPa for travertines and 15–45 MPa for carbonate tufas. Porosity strongly influences on travertine and tufas strength (Fig. 2b). The relationship between strength and porosity shows an exponential trend. In travertines with low poros-ity (non-porous travertines), a small change in the poros-ity causes great changes in rock strength. This trend is well established and is in concordance with previous studies (Jackson et al. 2005; Yagiz 2006; Török 2006; Demirdag 2009; Akin 2010; Akin and Özsan 2011; Garcia-del-Cura et al. 2012; Martinez-Martinez et al. 2013; Chentout et al. 2015; Sengun et al. 2015). Garcia-del-Cura et al. (2012) concluded that slope change in the strength–porosity plot for connected porosity values of ~ 10% (in their study total porosity was 13%) is related to a change in the characteris-tics of the porous system. On the one hand, at low porosity values, strength changes are due to the content of intercrys-talline and intergranular (interparticle) pores. Their influ-ence on mechanical properties is crucial due to the two-dimensional shape, which causes a stress concentration at their tips [according to the Griffith theory (Griffith 1921)]. This theory also argues that stress concentration increases as pore size increases (Fig. 1). On the other hand, at high porosity values, rocks present a variable content of vuggy macropores. They present a rounded geometry and stress concentration at their tips is lower than for interparticles pores, although they contribute to a surface reduction in the loaded sample section.

In general, the mechanical properties of the studied trav-ertines and tufas do no present a strong anisotropy and they behave according to the predominant rock facies. These results are in concordance with previous studies (Jack-son et al. 2005; Yagiz 2006; Garcia-del-Cura et al. 2012; Martinez-Martinez et al. 2013; Sengun et al. 2015). Thus, laminated travertines with low-porous facies show the high-est strength when the rock is tested perpendicular to load direction, whereas porous facies are stronger when the lami-nate is parallel to the load. The influence of structure on the mechanical anisotropy is not determinant in carbonate tufas. Results present an important dispersion because they have a complex and heterogeneous structure, and therefore, the role of the macrospores orientation on the mechanical anisotropy cannot be clearly evaluated.

Durability: evolution of the microstructural and petrophysical properties

Tables 2 and 3 and Fig. 3 display the evolution of petro-physical and durability properties after the durability tests. In general, travertines and carbonate tufas present an excel-lent durability against ice and salt crystallisation, compared to carbonates rocks with similar porosity values (Benavente et al. 2007a, b; Martinez-Martinez et al. 2013). They display unweathered aspect at mesoscale, although some samples undergo different types of weathering patterns. All samples display a superficial granular disaggregation, which contrib-utes to weight loss after the durability test. In laminated rocks, some superficial scaling is observed, which compro-mises loosing thick sheets of rock parallel to sample sur-faces. Fractures are scarce and occur parallel to the lamina-tion (in laminated travertines). NPM travertines present the best durability properties and remain nearly unweathered. However, laminated travertines with oxides in the vuggy porosity present a catastrophic decay. The presence of these oxides in vuggy porosity reduces the union strength between pore walls and therefore acts as a weakness plane under ice and salt crystallisation pressure. In particular, three samples from coloured travertines presented an important amount of oxides and underwent a breakdown before 48th cycle in the freeze–thaw test and before 14th cycle in the salt crystallisa-tion test (Fig. 4). This alteration pattern was also reported by Akin and Özsan (2011) in similar coloured travertines. The rest of the coloured travertine samples with fewer amounts of oxides did not suffer a breakdown. Moreover, two samples of the HT variety also suffered a breakdown in the 48th and 75th cycle, respectively, and petrophysical properties were not recorded.

SEM observations show the microstructural evolution of these stones caused by the ice and salt crystallisation (Fig. 5). Although travertines and tufas remained stable during durability tests, they underwent microcracking pro-cesses mainly related to both thermal stresses and mechani-cal pressures caused by the ice and salt crystallisation into pore space. There is a feedback between both decay mecha-nisms. Thermal stress can become crucial in carbonate rocks (Siegesmund and Dürrast 2011) under thermal cycles. Thus, temperature variation between different stages in salt crystal-lisation and freeze–thaw tests is, respectively, 40 and 32 °C. On the other hand, calcite has a highly anisotropic thermal dilatation, with a large dilatation coefficient along its crystal-lographic *c* axis and a strong contraction along *a* and *b* axes (Nye 1972). Therefore, crystals expand in one direction and contract along with other ones at the same time when they are heated. Thermally induced microcracking appears due to competing thermal expansion of different minerals that con-centrate on crystalline boundaries, especially in low-porosity stones (Gomez-Heras et al. 2009).

Table 2 Evolution of the petrophysical properties after the salt crystallisation test

	N_C	CT	HT	Lmix	NPCL	NPM	PL
P (%)	0	17.53 ± 7.25	39.78 ± 2.41	11.38 ± 2.91	7.41 ± 1.75	8.23 ± 1.97	22.51 ± 2.08
	15	17.94 ± 7.17	39.56 ± 2.32	13.17 ± 5.08	7.64 ± 1.61	8.28 ± 2.10	23.33 ± 2.57
	30	16.80 ± 7.70	40.28 ± 2.27	10.56 ± 3.25	6.26 ± 0.97	7.23 ± 1.73	21.48 ± 2.74
C_{par} (g/m^2 s$^{0.5}$)	0	26.23 ± 17.57	238.07 ± 93.58	7.59 ± 4.59	3.50 ± 2.26	4.47 ± 3.49	60.33 ± 35.42
	15	29.18 ± 16.97	258.99 ± 175.49	13.59 ± 10.38	5.68 ± 2.75	7.61 ± 3.12	60.01 ± 52.50
	30	31.88±19.74	302.21±148.37	24.05±35.62	5.57±1.14	10.22 ± 4.38	48.00 ± 14.13
A_C	0	0.76 ± 0.25	0.39 ± 0.29	0.40 ± 0.07	0.57 ± 0.21	0.71 ± 0.28	0.14 ± 0.10
	15	0.75 ± 0.19	0.27 ± 0.19	0.38 ± 0.09	0.66 ± 0.15	0.74 ± 0.24	0.34 ± 0.29
	30	0.67 ± 0.15	0.35 ± 0.15	0.38 ± 0.18	0.80 ± 0.16	0.76 ± 0.20	0.45 ± 0.24
v_P (m/s)	0	5305 ± 372	4016 ± 140	5575 ± 261	4150 ± 1315	5486 ± 168	4757 ± 173
	15	4942 ± 422	3734 ± 108	5242 ± 391	3202 ± 1853	4523 ± 519	4619 ± 247
	30	4858 ± 573	3754 ± 112	5107 ± 336	2993 ± 1777	3878 ± 816	4900
A_{vp}	0	0.97 ± 0.02	0.94 ± 0.03	0.92 ± 0.04	0.89 ± 0.07	0.95 ± 0.04	0.86 ± 0.06
	15	0.97 ± 0.03	0.93 ± 0.02	0.89 ± 0.08	0.87 ± 0.08	0.92 ± 0.05	0.85 ± 0.06
	30	0.96 ± 0.03	0.93 ± 0.03	0.90 ± 0.06	0.89 ± 0.06	0.85 ± 0.07	0.86
ΔW (%)	15	0.15 ± 0.11	0.97 ± 0.22	0.11 ± 0.08	0.03 ± 0.01	0.06 ± 0.16	0.14 ± 0.07
	30	0.57 ± 0.41	2.42 ± 0.64	0.61 ± 0.42	0.56 ± 0.46	0.21 ± 0.22	0.80 ± 0.63
σ_C (MPa)	0	37.46 ± 28.87	30.95 ± 11.12	59.80 ± 26.34	41.97 ± 11.15	37.40 ± 9.95	19.32 ± 0.74
	30	32.14 ± 1.58	28.27 7.71	38.35 ± 15.29	42.10 ± 31.07	65.86 ± 17.82	12.57 ± 0.63
n		7	6	9	8	19	5

Mean values and standard deviations for of the effective porosity. Facies: non-porous massive travertine (NPM), porous laminated travertine (PL), laminated with vugs and non-porous levels (Lmix) and non-porous cryptolaminated travertine (NPCL). Carbonate tufas have two facies, denominated as homogeneous (HT) and complex tufas (CT)

P capillary absorption coefficient in the direction parallel to the bedding, C_{par}, capillary anisotropy coefficient, A_C ultrasonic wave velocity, v_P anisotropy coefficient of v_P, A_{vp} dry weight loss, ΔW (%), compressive strength, σ_C number of cycles, N_C and number of tested samples

Both porosity and pore size distribution affect salt crystallisation and freeze–thaw durability. In general, travertines with low porosity values are more durable than porous travertine and tufas (Tables 2 and 3). Porosity contributes to the pore connectivity coordination and mechanical properties. Below 10% of connected porosity, pore connectivity dramatically decreases as a result of the closure and elimination of the throats; meanwhile, in rocks where porosity is higher than 10%, pore space is well con-nected and pore size distribution becomes the most impor-tant microstructure parameter (Benavente et al. 2007b, 2015). Figure 1 displays the influence between pore size distribution and pressure by ice and salt crystallisation. Benavente (2011) and Benavente et al. (2011) established that the effectiveness of crystallisation pressure generated by salt growth might be considered for the pore size range between 0.1 and 10 μm. The effectiveness of salt and ice pressure considerably decreases out of this pore interval. On the one hand, a crystal requires a considerable super-saturation to enter into the pore fraction below 0.1 μm, which is unlike when the stone is placed in the building. On the other, crystals may percolate through large pores without generating significant levels of crystallisation pressure on pore walls.

As a result, travertines and tufas undergo a very low weight loss in all varieties and durability tests, although the weight loss values are slightly higher in the salt crystallisation test (Tables 2, 3). The effective porosity variation is scarce during weathering. Surface weight loss and the appa-rition of microcracks do not change substantially the total void volume of the rocks. Benavente et al. (2007b) point out those fissures of varying widths and lengths may contribute to the detachment and fragmentation process. In particular, narrow micro-fissures appear to be important in the decay process due to the effectiveness of crystallisation pressure generated by salt growth. These internal microcracks may coalesce and then turn into macro-cracks and cause sample disintegration and scaling and even a catastrophic breakage in an interval of a very few number of cycles (Martinez-Martinez et al. 2013).

The variation of capillary absorption coefficient and the capillary anisotropy index, A_C, after durability tests is low. Tables 2 and 3 show the capillary absorption coefficient in the parallel direction to the lamination, C_{par}, which is the most sensible direction to the changes in pore structure. Figure 5b displays the development of microcracks in the parallel direction to the lamination and fenestral porosity. A_C quantifies the ratio of capillary coefficients in the parallel

Table 3 Evolution of the petrophysical properties after the freeze–thaw durability test

	N_C	CT	HT	Lmix	NPCL	NPM
P (%)	0	12.83 ± 7.85	34.05 ± 1.90	7.00 ± 3.97	6.20 ± 0.24	10.07 ± 2.19
	48	12.99 ± 7.71	30.55 ± 0.25	7.01 ± 4.00	6.46 ± 0.20	11.96 ± 5.26
	75	13.16 ± 7.95	31.41 ± 0.42	7.01 ± 4.03	6.36 ± 0.17	9.22 ± 1.34
	100	13.57 ± 8.40	32.92 ± 0.47	7.17 ± 4.11	6.67 ± 0.10	9.35 ± 1.24
C_{par} (g/m^2 s$^{0.5}$)	0	14.35 ± 13.76	397.62 ± 136.35	2.70 ± 0.66	3.77 ± 0.57	8.78 ± 6.28
	48	15.63 ± 16.25	416.25 ± 81.91	4.35 ± 2.65	1.96 ± 0.66	8.98 ± 7.27
	75	6.38 ± 5.42	156.97 ± 6.32	3.21 ± 1.36	1.88 ± 0.22	4.19 ± 1.20
	100	19.53 ± 21.17	93.15 ± 31.57	4.05 ± 1.39	3.61 ± 0.39	10.21 ± 12.09
A_C	0	0.70 ± 0.17	0.11 ± 0.03	0.72 ± 0.11	0.31 ± 0.02	0.71 ± 0.39
	48	0.92 ± 0.08	0.09 ± 0.01	0.74 ± 0.19	0.79 ± 0.12	0.79 ± 0.15
	75	0.48 ± 0.17	0.25 ± 0.01	0.86 ± 0.11	0.81 ± 0.23	0.67 ± 0.36
	100	0.80 ± 0.20	0.32 ± 0.08	0.80 ± 0.17	0.68 ± 0.10	0.72 ± 0.17
v_P (m/s)	0	5585 ± 378	4387 ± 335	5898 ± 289	3467 ± 270	5613 ± 88
	48	5496 ± 431	4023 ± 157	5865 ± 330	2854 ± 180	5492 ± 122
	75	5497 ± 341	4195 ± 130	5914 ± 213	2762 ± 126	5463 ± 145
	100	5501 ± 364	4277 ± 10	5819 ± 341	2723 ± 191	5369 ± 247
A_{vp}	0	0.97 ± 0.03	0.93 ± 0.03	0.97 ± 0.02	0.86 ± 0.01	0.97 ± 0.02
	48	0.97 ± 0.03	0.95 ± 0.00	0.98 ± 0.02	0.87 ± 0.04	0.95 ± 0.03
	75	0.97 ± 0.02	0.32 ± 0.16	0.97 ± 0.02	0.83 ± 0.01	0.95 ± 0.04
	100	0.97 ± 0.02	0.94 ± 0.05	0.97 ± 0.03	0.88 ± 0.03	0.93 ± 0.04
α_s (dB/cm)	0	6.94 ± 4.30	13.63 ± 0.53	3.17 ± 1.36	5.82 ± 0.55	4.89 ± 0.48
	75	6.91 ± 4.27	10.14 ± 5.17	2.79 ± 0.83	8.62 ± 0.25	4.88 ± 2.13
	100	6.59 ± 3.65	14.00 ± 0.11	3.65 ± 1.77	7.69 ± 0.98	6.26 ± 3.66
ΔW (%)	48	0.15 ± 0.04	0.49 ± 0.31	0.12 ± 0.06	0.01 ± 0.01	0.19 ± 0.10
	75	0.23 ± 0.12	1.12 ± 0.21	0.12 ± 0.06	0.02 ± 0.00	0.19 ± 0.10
	100	0.35 ± 0.21	1.71 ± 0.19	0.14 ± 0.07	0.03 ± 0.00	0.21 ± 0.11
σ_C (MPa)	0	43.39 ± 27.56	30.95 ± 11.12	57.13 ± 9.23	45.42 ± 0.00	38.79 ± 10.70
	100	45.54 ± 27.63	8.92 ± 1.72	77.90 ± 44.08	17.58 ± 2.91	60.28 ± 23.50
n		6	4	4	4	4

Mean values and standard deviations for of the effective porosity. Facies: non-porous massive travertine (NPM), laminated with vugs and non-porous levels (Lmix) and non-porous cryptolaminated travertine (NPCL). Carbonate tufas have two facies, denominated as homogeneous (HT) and complex tufas (CT)

P capillary absorption coefficient in the direction parallel to the bedding, C_{par} capillary anisotropy coeffi-cient, A_C ultrasonic wave velocity, v_P anisotropy coefficient of v_P, A_{vp} spatial attenuation, α_s dry weight loss, ΔW (%) compressive strength, σ_C number of cycles, N_C and number of tested samples

and perpendicular direction. In the salt durability test (the most aggressive test), the capillary coefficients show a slight increase, mainly in the last cycle (30th cycle). This occurs because in the 15th cycle salt is not completely removed from the sample. Consequently, this fraction of salt, which fills pores and microcracks, does not contribute to capillary flow. As we described in “Materials and methods” section, samples were cleaned after the 30th cycle. This scarce variation reveals that the internal microcracks produced by the crystallisation pressure present little connection (Fig. 5a), and therefore, they do not enhance noticeably the water flow. Travertines and tufas present a low-to-medium mechani-cal resistance. This mechanical behaviour of rocks also contributes to their durability against salt crystallisation and freeze–thaw cycles. The susceptibility of the porous rock to the ice and salt crystallisation mechanism is closely connected to its strength. It is the material’s resistance to crystallisation pressure, which creates tensile stress over the pore surface (Benavente et al. 2004; Coussy 2005, 2006). The mechanical strength evolution is scarce after durability tests, and in most of the cases, its variation ranges between the maximum and minimum resistance of the unweathered samples (Fig. 3). As described above, microcracks appear inside of rocks at the microscale and they are not enough to cause mechanical decay of rocks.

Mechanical variation corroborates that salt crystallisation test is more aggressive than freeze–thaw test. Mechani-cal strength of NPCL, Lmix and HT slightly decreases, CT remains nearly unweathered, whereas PL and NPM traver-tines seem to undergo an improvement of the mechanical

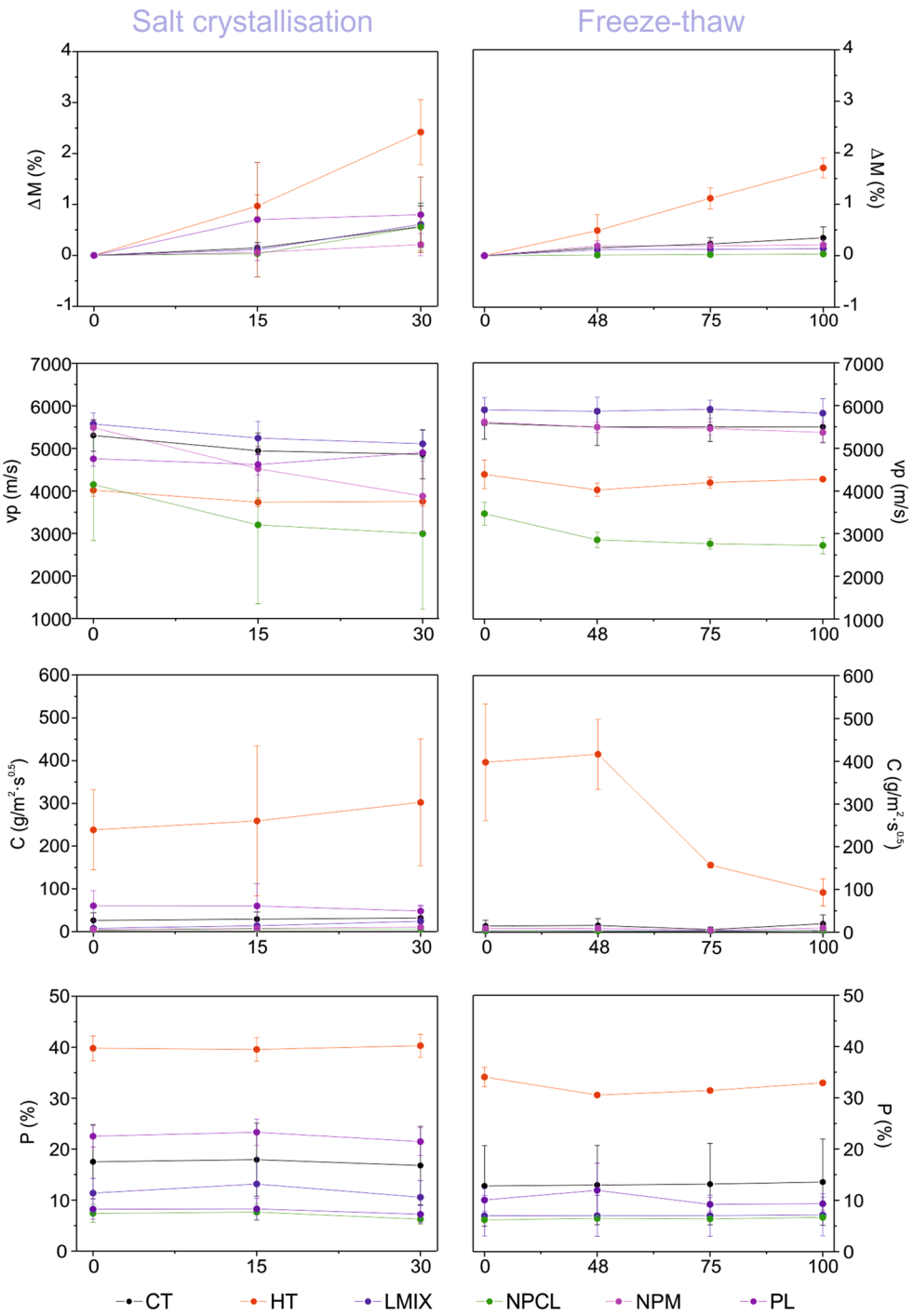

Fig. 3 Evolution of physical properties of travertines and carbonate tufas during the salt crystallisation and freeze–thaw durability tests

properties. This improvement can be related to the so-called ageing of the testing sample. This can be explained by the relaxation reaction phenomenon of the rocks after they have been removed from the quarry and exposed to chang-ing environmental conditions (pressure, temperature and moisture) (Siegesmund and Dürrast (2011) and references herein).

Tables 1 and Fig. 2 highlight the ultrasonic wave velocity (v_P) and spatial attenuation (α_S) values for the unweathered samples and their relationship with porosity, and Tables 2 and 3 and Fig. 3 display their evolution during the durability tests. Samples with low wave velocities and high attenuation values present higher deterioration levels. v_P and α_S depend mainly on pore structure and reflect the durability properties of rocks. For example, HT presents high effective porosity values and large pore sizes, which provide low values of v_P (around 4100 m/s) and high values of α_S (over 13 dB/cm). v_P slightly decreases as the number of cycles, and it is related

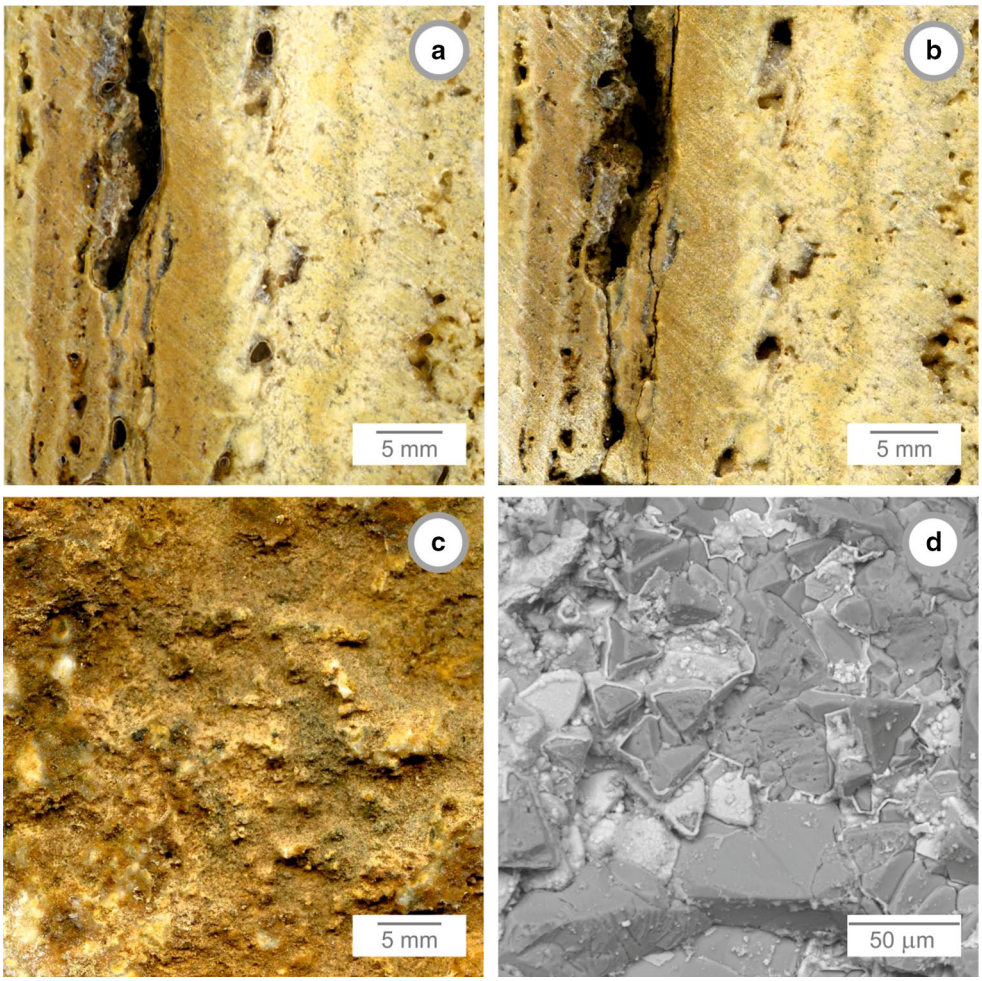

Fig. 4 Catastrophic breakage of a coloured travertine with an important amount of oxides in the vuggy porosity. Aspect of the **a** unweathered sample, **b** weathered sample after 14th cycle in the salt crystallisa-tion test. **c** Photograph of the oxides on the vuggy porosity, **d** morphology of the Fe–Mn oxyhydroxides under SEM-bse

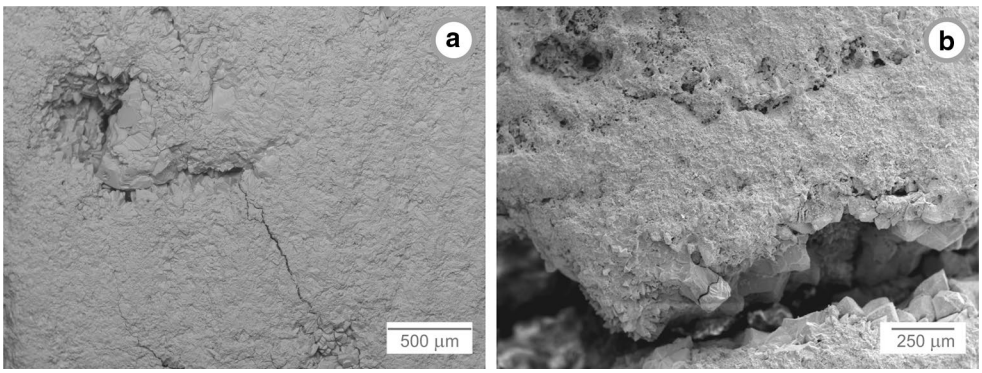

Fig. 5 Examples of microstructural evolution of weathering sam-ples (SEM-bse images). Microstructural features of a porous lami-nated travertine caused by salt crystallisation under scanning electron

to the microstructural weathering suffered in travertines and tufas. As we discussed above, salt crystallisation and freeze–thaw test comprise salt or ice pressures and thermal stress and, as a consequence, the development of microc-racks in the samples. The evolution of the spatial attenuation was also recorded in the freeze–thaw test and presents a microscopy. a Microcracks caused by the crystallisation pressure and porosity connection by the microcracks. **b** Development of microc-racks parallels to the lamination and fenestral porosity

slight increment during the durability cycles. Therefore, the scarce evolution of the ultrasonic parameters corroborates the number and development degree of internal microcracks is not enough to internally deteriorate the rocks.

Bulk properties of travertines and carbonate tufas remain unchanged after a long number of cycles, which highlights

their excellent durability properties. In fact, the number of cycles in the salt crystallisation standard test is 15 and, in this paper, we performed 30 cycles; in the freeze–thaw test, samples underwent 100 cycles, which exceeds the com-mon number for the durability characterisation of building stones. However, catastrophic decay is a nonlinear process that tested samples might suffer. The initial microcracks may grow and become to coalesce. Consequently, sample can breakdown in a few cycles. Smith et al. (2008) argued that this situation constitutes the critical threshold for mac-roscopic decay initiation. When this critical threshold is exceeded, microcracks turn into cracks and grow rapidly. The increase in porosity may accelerate the decay process until the ultimate failure is reached in very few cycles (Mar-tinez-Martinez et al. 2013).

Conclusions

In this paper, we studied a representative number of traver-tine textures, which include non-porous massive, non-porous cryptolaminated, porous laminated and laminated with vugs and non-porous levels. In addition, we also studied various carbonate tufas ranging from homogeneous to complex tex-tures. Results demonstrate that the studied travertines and carbonate tufas exhibit a very high durability against salt and ice crystallisation cycles, compared to carbonates rocks with similar porosity values. The evolution of petrophysical properties was slightly more intensive after 30 cycles of salt crystallisation than 100 cycles of freeze–thaw.

In general terms, samples displayed unweathered aspect at mesoscale, although some of them underwent different types of weathering patterns with low intensity. All samples displayed a superficial granular disaggregation, which con-tributed to weight loss after the durability test. Laminated rocks suffered some superficial scaling. Remarkably, some laminated travertine samples with an important amount of oxides in the vuggy porosity presented a catastrophic decay. In this situation, the presence of these oxides in vuggy porosity reduces the union strength between pore walls and therefore acts as a weakness plane under ice and salt crystal-lisation stresses.

Porosity fraction and the manner in which the vugs are connected affected the petrophysical and durability proper-ties of the travertines and carbonate tufas. In the travertine facies, vuggy macropores can be considered as separate-vug porosity. Their addition to interparticle porosity increases effective porosity and reduces their mechanical strength but does not significantly increase capillary transport and the effectiveness to salt and ice pressures. In the carbonate tufa, vuggy pores act as touching-vug pores. Travertines and carbonates tufas with the highest effective porosity values (> 10%) were the least durable because pore connectedness increases and mechanical strength decreases with the porosity.

The microstructure analysis under scanning electron microscopy revealed that they underwent microcracking processes related mainly to both thermal stresses and/or ice and salt pressures. Microcracks presented little connection, and they did not enhance noticeably to the water flow or decrease the mechanical properties.

From this investigation, we can conclude that travertines and carbonate tufas are appropriate as a construction and building material. Particular attention must be paid to estab-lish the direction of stone cutting and its relative placement in the building for samples with strong anisotropic properties and also to the presence of abundant amount of oxides in the vuggy porosity.

Acknowledgements

This study was financed by the Spanish Minis-try of Education and Science (MEC) through the Research Project CGL2006-05027/BTE and Community of Madrid (S2023/MIT 2914). A pre-doctoral research fellowship was awarded to N. Cueto by the MEC. We sincerely thank to C. Pla for her invaluable help and sugges-tions for improving the manuscript.

References

Akin M (2010) A quantitative weathering classification system for yel-low travertines. Environ Earth Sci 61:47–61

Akin M, Özsan A (2011) Evaluation of the long-term durability of yel-low travertine using accelerated weathering tests. Bull Eng Geol Environ 70:101–114

Benavente D (2011) Why pore size is important in the deterioration of porous stones used in the built heritage? Macla 15:41–42

Benavente D, Garcia-del-Cura MA, Fort R, Ordoñez S (2004) Durabil-ity estimation of porous building stones from pore structure and strength. Eng Geol 74:113–127

Benavente D, Cueto N, Martinez-Martinez J, Garcia-del-Cura MA, Cañaveras JC (2007a) The influence of petrophysical proper-ties on the salt weathering of porous building rocks. Env Geol 52:197–206

Benavente D, Martinez-Martinez J, Cueto N, Garcia-del-Cura MA (2007b) Salt weathering in dual-porosity building dolostones. Eng Geol 94:215–226

Benavente D, Sanchez-Moral S, Fernandez-Cortes A, Cañaveras JC, Elez J, Saiz-Jimenez C (2011) Salt damage and microclimate in the Postumius Tomb, Roman Necropolis of Carmona, Spain. Envi-ron Earth Sci 63:1529–1543

Benavente D, Pla C, Cueto N, Galvañ S, Martinez-Martinez J, Garcia-Del-Cura MA, Ordóñez S (2015) Predicting water permeability in sedimentary rocks from capillary imbibition and pore structure. Eng Geol 195:301–311

Chentout M, Allou B, Rezouk A, Belhai D (2015) Experimental study to evaluate the effect of travertine structure on the physical and mechanical properties of the material. Arab J Geosci 8:8975–8985

Choquette PW, Pray LC (1970) Geology nomenclature and clas-sification of porosity in sedimentary carbonates. AAPG Bull 54:207–250

Coussy O (2005) Poromechanics of freezing materials. J Mech Phys Solids 53:1689–1718

Coussy O (2006) Deformation and stress from in-pore drying-induced crystallization of salt. J Mech Phys Solids 54:1517–1547

Curie J (2013) Les travertins anthropiques, entre histoire, archéologie et environnement: étude geoarchéologique du site antique de Jebel Oust (Tunisie). Dissertation, Université de Bourgogne

Deere DU, Miller RP (1966) Engineering classification and index properties for intact rock. Air Force Weapons Laboratory Technical, Report AFWL-TR-65-116

Demirdag S (2009) The effect of using different polymer and cement based materials in pore filling applications on technical parameters of travertine stone. Constr Build Mater 23:522–530 Demirdag S (2013) Effects of freezing–thawing and thermal shock cycles on physical and mechanical properties of filled and unfilled travertines. Constr Build Mater 47:1395–1401

Ford TD, Pedley HM (2006) A review of tufa and travertine deposits of the world. Earth Sci Rev 41:117–175

Garcia-del-Cura MA, La Iglesia A, Benavente D, Bernabeu A, Gonzalez-Martin JA (2007) Mineralogía de los travertinos pleistocenos de Albox (Almeria), importante recurso de materia prima de rocas ornamentales. Macla 7:89

Garcia-del-Cura MA, La Iglesia A, Ordoñez S, Sanz-Montero ME, Benavente D (2008) Óxidos de hierro y manganeso en travertinos de Alhama de Almería. Macla 9:107–108

Garcia-del-Cura MA, Benavente D, Martinez-Martinez J, Cueto N (2012) Sedimentary structures and physical properties in trav-ertine and carbonate tufa building stone. Constr Build Mater 28:456–467

Garcia-del-Cura MA, Benavente D, Martinez-Martinez J (2014) La tobas: un recurso pétreo. In: Gonzalez Martin JA, Gonzalez Amuchastegui MJ (eds) Las Tobas en España. Sociedad Española de Geomorfología, pp 349–355

Garcia-del-Cura MA, Benavente D, Martinez-Martinez J, Ordoñez S (2017) Travertinos coloreados en la Cordillera Bética (SE de la Península Ibérica). Situación geológica y características petrofísi-cas. Bol Geol Min 127:467–483

Gomez-Heras M, McCabe S, Smith BJ, Fort R (2009) Impacts of fire on stone-built heritage an overview. J Architect Conserv 15:47–58 Griffith AA (1921) The phenomena of rupture and flow in solids. Philos Trans R Soc Lond A 221:163–198

Jackson MD, Marra F, Hay RL, Cawood C, Winkler EM (2005) The judicious selection and preservation of tuff and travertine building stone in ancient Rome. Archaeometry 47:485–510

Lucia FJ (1995) Rock-fabric petrophysical classification of carbonate pore-space for reservoir characterization. AAPG Bull 79:1275–1300

Martinez-Martinez J, Benavente D, Garcia-del-Cura MA (2011) Spatial attenuation: the most sensitive ultrasonic parameter for detecting petrographic features and decay processes in carbonate rocks. Eng Geol 19:84–95

Martinez-Martinez J, Benavente D, Gomez-Heras M, Marco-Castaño L, Garcia-del-Cura MA (2013) Non-linear decay of building stones during freeze–thaw weathering processes. Constr Build Mater 38:443–454

Martinez-Martinez J, Fusi N, Galiana-Merino JJ, Benavente D, Crosta GB (2016) Ultrasonic and X-ray computed tomography characterization of progressive fracture damage in low-porous carbonate rocks. Eng Geol 200:47–57

Nye JF (1972) Physical properties of crystals. Oxford University Press, London

Pedley M (2009) Tufas and travertines of the Mediterranean region: a testing ground for freshwater carbonate concepts and developments. Sedimentology 56:221–246

Pentecost A (2005) Travertine. Springer-Verlag, Berlin

Pentecost A, Viles HA (1994) A review and reassessment of travertine classification. Geogr Phys Quatern 48:305–314

Roduit N (2007) JMicroVision: image analysis toolbox for measuring and quantifying components of high-definition images. Version 1.27. http://www.jmicrovision.com. Accessed 23th Oct 2017 Sanchez-Moral S, Luque L, Cuezva S, Soler V, Benavente D, Laiz L, Gonzalez JM, Saiz-Jimenez C (2005) Deterioration of building materials in Roman catacombs: the influence of visitors. Sci Total Environ 349:260–276

Sengun N, Demirdag S, Ugur I, Akbay D, Altindag R (2015) Assessment of the physical and mechanical variations of some travertines depend on the bedding plane orientation under physical weather-ing conditions. Constr Build Mater 98:641–648

Siegesmund S, Dürrast H (2011) Physical and mechanical properties of rocks. In: Siegesmund S, Snethlage R (eds) Stone in architecture. Springer, Berlin

Smith BJ, Gomez-Heras M, McCabe S (2008) Understanding the decay of stone-built cultural heritage. Prog Phys Geog 32:361–439

Soete J, Kleipool LM, Claes H, Claes S, Hamaekers H, Kele S, Ozkul M, Foubert A, Reijmer JJG, Swennen R (2015) Acoustic proper-ties in travertines and their relation to porosity and pore types. Mar Pet Geol 59:320–335

Török A (2006) Hungarian travertine: weathering forms and durability. In: Fort R, Alvarez de Buergo M, Gómez-Heras M, Vazquez-Calvo C (eds) Heritage, weathering and conservation. Taylor & Francis Group, London, pp 199–204

Török A, Vasarhelyi B (2010) The influence of fabric and water content on selected rock mechanical parameters of travertine, examples from Hungary. Eng Geol 115:237–245

UNE-EN 12370 (1999) Natural stone test methods. Determination of resistance to salt crystallisation. European Committee for Standardization, Bruxelles

UNE-EN 12371 (2011) Natural Stone tests methods. Determination of frost resistance. European Committee for Standardization, Bruxelles

UNE-EN 1925 (1999) Natural stone test methods. Determination of water absorption coefficient by capillarity. European Committee for Standardization, Bruxelles

UNE-EN 1926 (2007) Natural stone tests methods. Determination of uniaxial compressive strength. European Committee for Standardization, Bruxelles

UNE-EN 1936 (2007) Apparent and real density, and open and total porosity. European Committee for Standardization, Bruxelles

Unterwurzacher M, Obojes U, Hofer R, Mirwald M (2010) Petrophysical properties of selected Quaternary building stones in western Austria. In: Pøikryl R, Török A (eds) Natural stone resources for historical monuments. Geological society, vol 333. Special Publications, London, pp 143–152

Urosevic M, Sebastian-Pardo E, Cardell C (2010) Rough and polished travertine building stone decay evaluated by a marine aerosol ageing test. Constr Build Mater 24:1438–1448

Yagiz S (2006) Overview on geo-mechanical assessments of Denizli travertines in Turkey. Book of abstracts. In: 10th international association for engineering geology congress, Nottingham 2006. Paper number 384

Yavuz AB, Topal T (2007) Thermal and salt crystallisation effects on marble deterioration: examples from Western Anatolia, Turkey. Eng Geol 90:30–40

Yu S, Oguchi CT (2010) Role of pore size distribution in salt uptake, damage, and predicting salt susceptibility of eight types of Japa-nese building stones. Eng Geol 115:226–236

Zalooli A, Khamehchiyan M, Nikudel MR, Jamshidi A (2017) Deterio-ration of travertine samples due to magnesium sulfate crystallisa-tion pressure: examples from Iran. Geotech Geol Eng 35:463–473